JOURNAL OF GAS TECHNOLOGY

Volume 9 / Issue 1 / Summer 2024 / Pages 5-18

Journal Home page: http://jgt.irangi.org

Evaluation of the Impact of Aqueous Phase Salinity on Carbon Dioxide Mineralization during Gas Sequestration

Bright Bariakpoa Kinate[1*], Ugwunna Dickson Amadi[2], Olalekan Kunle Akindele[3], Jeremiah Ifeanyi Okoroma[4]

1,4. Department of Petroleum Engineering, Rivers State University, Port Harcourt, Nigeria
2. Department of Petroleum and Gas, University of Salford, Manchester, UK
3. Department of Data Science, Artificial Intelligence and Modeling, University of Hull, UK

ARTICLE INFO

ORIGINAL RESEARCH ARTICLE

Article History:
Received: 12 July 2024
Revised: 17 August 2024
Accepted: 23 August 2024

Keywords:
Mineralization
Dissolution
Aquifer model
Phase Salinity
Sequestration

DOR: 20.1001.1/jgt.2024.2033713.1042

ABSTRACT

Aqueous phase salinity has a major effect on the quantity of carbon dioxide trapped by solubility trapping and may also affect mineral dissolution and precipitation. While carbon dioxide storage through structural, residual, dissolution and partly mineral trapping modes have a wide investigation, the mineral trapping potential and its influencing factors have not been explored. In this work, the effects of variable aqueous phase salinity on carbon dioxide mineralization were investigated. Numerical simulations were done using a geochemical simulator and three-dimensional homogeneous aquifer model of dimensions 30×30×10 (9000 grid blocks) and block width of 70 m was built. The generated grid was populated with petrophysical, grid and rock properties .Four models with similar rock and fluid characteristics were simulated for pure water and different salinity of 0.01 wt (10000 ppm), 0.015 wt (15000 ppm) and 0.02 wt (20000 ppm) respectively. Result shows a decrease in the moles of carbon dioxide solubilized with an increase in brine salinity level. Increase in brine salinity decreases the moles of carbon dioxide converted to aqueous ions and dissolution in resident brine. There was an increase in the rate of Kaolinite precipitation, Calcite precipitation and a decrease in the rate of Anorthite dissolution with increase in duration of carbon dioxide injection. The mineral mole changes for Anorthite increases with level of salinity and decreases with duration of carbon dioxide injection. Moreover, Calcite and Kaolinite mineral moles changes decreases with level of salinity and with duration of carbon dioxide injection. Calcite and Kaolinite decreases as aqueous phase salinity increases. This work has shown that formation minerals has different reactivity to salinity concentration which decides carbon dioxide trapping and storage capacity.

How to cite this article
B.B. Kinate, U.D. Amadi, O.K. Akindele, J.I. Okoroma, Evaluation of the Impact of Aqueous Phase Salinity on Carbondioxide Mineralization during Gas Sequestration. Journal of Gas Technology. 2024; 9(1): 5 -18. (https://jgt.irangi.org/article_717199.html)

* Corresponding author.
E-mail address: kinate.bright@ust.edu.ng, (B.B. Kinate).

Available online 10 September 2024

1. Introduction

Carbon dioxide (CO_2) is the major greenhouse gas (GHG), that arises mostly from the consumption of fossil fuels. Indisputably, sensible environmental difficulties such as climate changes and an increase in the global surface temperature are as a result of a rise in carbon dioxide emission (Abas and Khan, 2014; Olajire, 2018; Venkatraman and Alsberg, 2017; Liu et al., 2018; Singh, 2018). Geological carbon storage is one of the most promising strategies to decrease anthropogenic carbon emissions by trapping the carbon dioxide from big stationary sources and depositing it into deep geological formations (Pruess et al., 2003).

Among the numerous sorts of prospective storage locations, saline aquifers have been identified with the biggest storage capacity(Zhang et al., 2016).Generally carbon dioxide should be injected at depths below 800 m, where formation temperature and pressure would preserve the carbon dioxide in a dense supercritical phase (Pruess et al., 2003; Pentland et al., 2011). The brine-carbon dioxide density difference can then migrate toward the surface vertically. The movement can be minimized and carbon dioxide can be inhibited from leaking to the atmosphere via four basic trapping strategies, namely structural trapping (Hesse et al., 2008; Naylor et al., 2011; Iglauer et al., 2015), residual trapping which relies on the capillary forces (Pentland et al., 2011; Iglauer et al., 2011; Krevor et al., 2015; Rahman et al., 2016), dissolution trapping (Spycher et al., 2003) which is a function of carbon dioxide-brine interfacial area (Kumar et al., 2005) and mineral trapping (Xu et al., 2004; Gaus, 2010) which is a factor of the chemical reactions between reservoir rock minerals,fluids and the injected carbon dioxide (Xu et al., 2003; 2005).

The permanent storage of carbon dioxide in saline aquifer is connected with mineral trapping (Pruess, 2003; Gunter et al., 2004), where dissolved carbon dioxide reacts with the minerals present in the formation rock and with cations present in the pore water to form stable mineral precipitates, which bind injected carbon dioxide more tightly into the aquifer.

These geo-chemical reactions becomes the trapping processes for the injected carbon dioxide in saline aquifers and rely on a number of parameters, including the existing pressure and temperature of the formation, the mineralogy of the formation rock and the composition and salinity of the resident brine (Gaus, 2010).

During carbon dioxide storage, solubility and mineral trapping processes are connected in which solubility in brine have an impact on the rate of mineral trapping. As example, the higher the solubility, the more carbon dioxide that can react with formation minerals (Bachu, 2016; Kolster et al., 2018). Significantly, brine salinity has an effect on the amount of carbon dioxide trapped by solubility trapping (Saraji et al., 2014; Al-Yaseri et al., 2016; Arif et al., 2016a) and may positively or negatively influence mineral dissolution and precipitation. Carbon dioxide solubility in brine has been shown to decrease with increase in brine salinity (Al-khdheeawi et al., 2017; Al-khdheeawi et al., 2018). Kumar et al. (2020) opined that increase in brine salinity decreases the storage efficiency and mass of carbon dioxide dissolved in the aqueous phase but no significance effect on mineral precipitation in carbonate formation.

The objective of this study is to analyze the impact of different brine salinity level on carbon dioxide dissolution, carbon dioxide aqueous ions, mineral moles changes, carbon dioxide trapped for different mineral types (Anorthite, Calcite, and Kaolinite). CMG-GEM was used to built a three dimensional geological model of the aquifer and PR1978 EOS used for the thermodynamic properties evaluation. An injector well was built and completed in three layers at the bottom of the model and shut in after 10 simulation years of carbon dioxide injection and fate monitored for 190 simulation years. Then, the base model for water with no salinity was initiated and three models simulated for three different salinities and compared for the carbon dioxide mineralized for three different mineral types.

2. Methodology

2.1.Simulation and Input Data

CMG simulator and data on Aquifer properties (Aquifer depth, thickness , width, and length, Rock compressibility, Initial temperature and pressure, Permeability and porosity), Rock physics functions (saturations and phase relative permeabilities), Fluid properties (Methane and Carbon dioxide fractions, Aquifer temperature, Aquifer salinity), Injection well (Grids well completion, Well radius and skin, Maximum Bottom-hole pressure, Maximum injection rate), Mineral properties and kinetic parameters (Rate constant, Reactive surface area, Activation energy, Molecular weight and initial volume fraction) were used and presented in (Table 1 to Table 6).

Table 1. Aquifer Properties for the Initial Condition (Khan et al., 2015)

Property	Value
Aquifer depth	1265 m
Aquifer thickness (z direction)	300 m (10×30)
Aquifer length	2100 m (30×70)
Rock compressibility	4.5×10^{-7} per kPa
Initial reservoir temperature	45 °C
Initial reservoir pressure	12400 kPa
Permeability	165 mD
Porosity	0.21
Gas/Water contact	1250 m

Table 2. Data for GEM Fluid Model Creation (Khan et al., 2015)

Component	Mole fraction
CH_4	0.999
CO_2	0.001
Aquifer temperature	45 °C
Aquifer salinity	10000 ppm (base case)

Table 3. Properties and Kinetic Rate Parameters for Minerals (Khan et al., 2015)

Minerals	Rate Constant mol/m². s	Reactive Surface Area m²/m³	Activation Energy J/mole	Molecular Weight g/mol	Initial Volume Fraction
Calcite	-8.78	88	41870	100	0.0088
Anorthite	-12	88	67830	278	0.0088
Kaolinite	-13	17600	62760	258.1603	0.0176

Table 4. Water Relative Permeability Data

Sw	Krw	Krow
0.20	0.0000	1.0000
0.30	0.0002	0.5862
0.40	0.0039	0.3164
0.50	0.0198	0.1526
0.60	0.0625	0.0625
0.70	0.1526	0.0198
0.8	0.3164	0.0039
0.9	0.5862	0.0002
1	1.0000	0.0000

Table 5. Gas Relative Permeability Data

Sg	Krg	Krog
0.05	0.0005	0.7725
0.1	0.0037	0.5862
0.2	0.0273	0.3164
0.3	0.0857	0.1526
0.4	0.1875	0.0625
0.5	0.3357	0.0198
0.6	0.5273	0.0039
0.7	0.7537	0.0002
0.8	1.0000	0.0000

Table 6. Parameters of the Injection Well (Khan et al., 2015)

Property	Value
Grids well completion (I J K)	15, 15, 8-10
Injection duration	10 years
Well radius	0.0762 m
Skin	0
CO_2 mole fraction	1
Maximum Bottom-hole Pressure	28300 kPa
Maximum injection rate (SC)	89200 m^3/day

2.2. Transport Equation for Mineral and Aqueous Phase

The simulations were performed using the commercial compositional generalised equation of state simulator (CMG-GEM). The governing equations are given in equation (1), (2), (3) and (4);

For the components of the gaseous phase, the mass balance equation is given by;

$$\frac{\partial N_{ig}}{\partial t} = \nabla.\left(\frac{\rho_g k k_{rg} m_{ig,g}}{\mu_g}\right)(\nabla p + \nabla p_{cwg} - \rho_g g \nabla z) + \nabla.\left(\frac{\rho_w k k_{rw} m_{ig,w}}{\mu_w}\right)(\nabla p + \nabla p_{cwg} - \rho_w g \nabla z) + \nabla. J_{ig} + \sigma_{ig,aq} + q \quad (1)$$

For the components in the aqueous phase;

$$\frac{\partial N_{ia}}{\partial t} = \nabla.\left(\frac{\rho_w k w m_{ia,w}}{\mu_w}\right)(\nabla p - \rho_w g \nabla z) + \nabla. J_{ia} + \sigma_{ia,aq} + \sigma_{ia,mn} + q \quad (2)$$

For the minerals;

$$\frac{\partial N_{km}}{\partial t} = \sigma_{km,mn} \quad (3)$$

Where $\sigma_{km,mn}$ is mineral reaction rate, ρ_g is density of gas, ρ_w is density of water, ρ_{cwg} is capillary pressure between water and gas, J_{ig} is diffusion/dispersion of gas component, J_{ia} is diffusion/dispersion of aqueous component, N_{ig} is the number of moles of gas component i per grid volume, q is well molar flow rate of gas component, $m_{ig,g}$ is the mole fractions of gas component i in gas phase, $m_{ig,w}$ is the mole fractions of gas component i in aqueous phase, $m_{ia,w}$ is mole fraction of aqueous component i in aqueous phase, $\sigma_{ig,aq}$ is reaction rate between gaseous and aqueous component, $\sigma_{ia,aq}$ is reaction rate between aqueous and aqueous component, $\sigma_{ia,mn}$ is reaction rate between aqueous and mineral component, k is permeability, k_{rg} is gas relative permeability, k_{rw} is water relative permeability, t is time step, and z is depth and p is water pressure.

The first terms at left hand side of equations (1), (2) and (3) represent the accumulation.

The first and second terms at the right-hand side of equations (2), and (3) describe convective and diffusive transport respectively. q in equations (1) and (2) are the flow rates and, in this study, represent the CO_2 injection rate.

The mineral dissolution/precipitation due to chemical reactions with the components forming the aqueous phase in equations (3) is governed by:

$$R_i = A_i k_i \left(\frac{1 - Q_i}{k_{eq,i}}\right) \quad (4)$$

Where A_i is reactive surface area for mineral i, k_i is reaction rate constant, Q_i is activity product of mineral reaction i, and $k_{eq,i}$ is the equilibrium constant for mineral reaction.

The numerical method adopted for solving the above governing equations was the finite difference method with the adaptive-implicit discretisation. Newton's method was used to solve the equations describing the flow, the phase equilibrium, the chemical equilibrium and the mineral dissolution and precipitation rates.

Geochemical reactions

i. Intra-aqueous chemical equilibrium reactions

$$CO_{2(aq)} + H_2O = H^+ + HCO_3^-$$

$$CO_3^{2-} + H^+ = HCO_3^-$$

$$OH^- + H^+ = H_2O$$

ii. Mineral reactions

$$Calcite + H^+ = Ca^{2+} + HCO_3^-$$

$$Anorthite + 8H^+ = Ca^{++} + 2Al^{+++} + 2SiO_{2(aq)} + 4H_2O$$

$$Kaolinite + 6H^+ = 5H_2O + 2SiO_{2(aq)} + 2Al^{+++}$$

$Koalinite: Al_2Si_2O_5(OH)_4$

$Calcite: CaCO_3$

$Anorthite: CaAl_2Si_2O_8$

2.3. Simulation Approach

We used CMG-GEM and built-in grid building module "Builder" to generate the geological model of the aquifer. A three (3) dimensional homogeneous aquifer model of dimensions 30×30×10 (9000 grid blocks) and block width of 70 m was built. The generated grid was populated with petrophysical, grid and rock properties with

the data presented in (Table 1). Data in (Table 2) and (Table 3) were used for the calculation of the properties of CH_4 and CO_2 (critical pressure, critical temperature, acentric factors and binary interaction coefficients) and the mineral species present in the aquifer at initial condition with PR1978 selected as the EoS for thermodynamic properties calculation. The aquifer was assumed to be completely saturated with reservoir brine and has an insignificant concentration of trace gas (methane gas). Li-Nghiem's model was used for the calculation of Henry's constant for gas solubility in brine. The created fluid model was imported into the component section of GEM data file. Relative permeability data in (Table 4) and (Table 5) were used to define the relative permeability curves and the model was initialized with water-gas contact set at 1250 m above the reference depth which gave a model fully saturated with brine. Gas cap was initialized with supercritical CO_2 fraction of 0.001 and CH_4 fraction of 0.999 respectively.

An injector well 'CO_2_INJECTOR' was completed in three layers at the bottom of the model with the data presented in (Table 6). Pure supercritical CO_2 was injected at a maximum, constant surface gas rate of 89200 m^3/day with a bottomhole injection pressure limit of 28300 kPa for 10 years. The injector was shut-in after 10 years of CO_2 injection with the CO_2 fate monitored for 190 years. The base case model for pure water (zero salinity level) was initiated and three models with similar rock and fluid characteristics simulated for different salinity of 0.01 wt (10000 ppm), 0.015 wt (15000 ppm) and 0.02 wt (20000 ppm) in terms of NaCl concentration as brines and modeled with assumption that the total salinity is due only to Na+ and Cl- ions. The simulation work flow is shown in (Figure 1).

The 3D visualization of the reservoir model for case with no salinity, 10000 ppm, 15000 ppm and 20000 ppm salinities are presented in (Figure 2), (Figure 3), (Figure 4) and (figure 5).

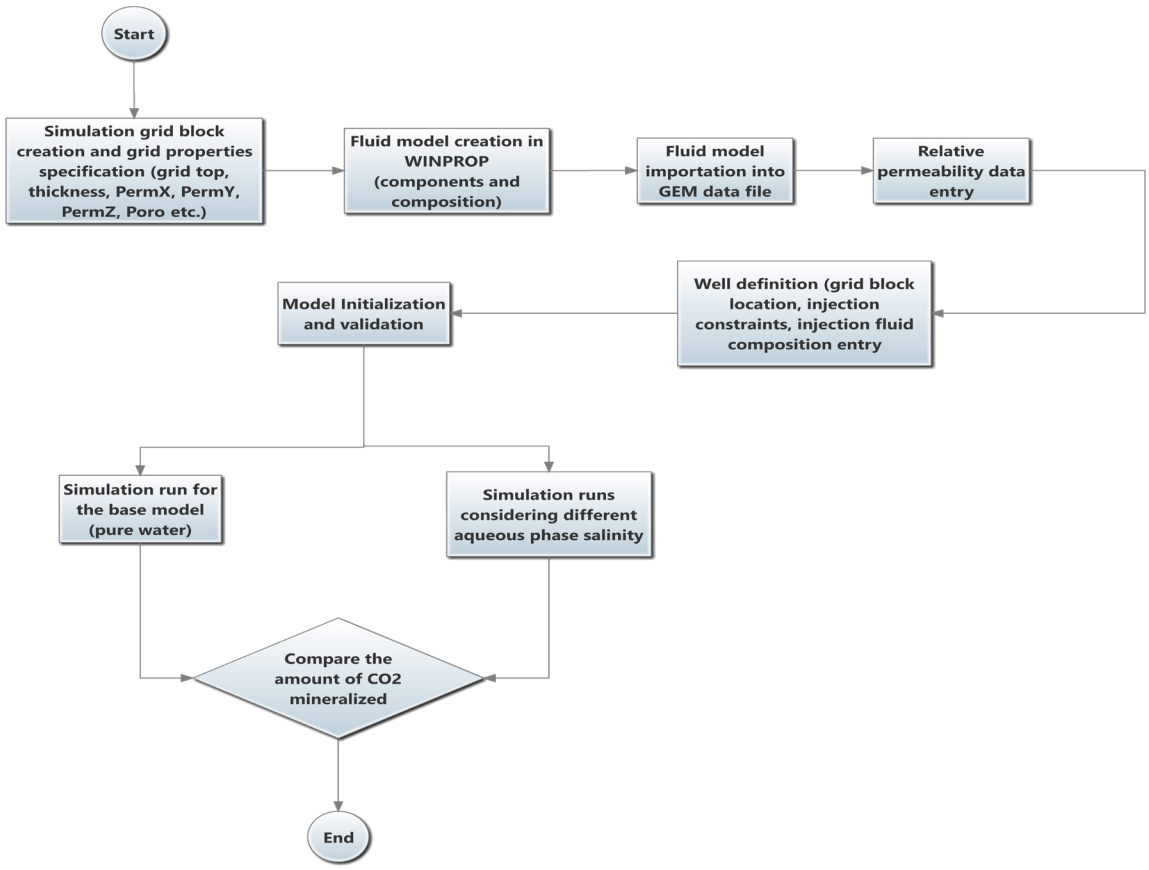

Figure 1. Simulation Work Flow

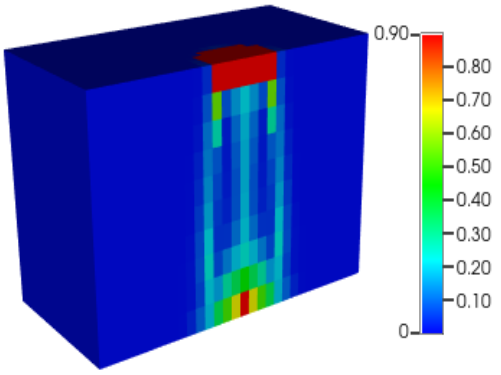

Figure 2. 3D Model for 0 ppm

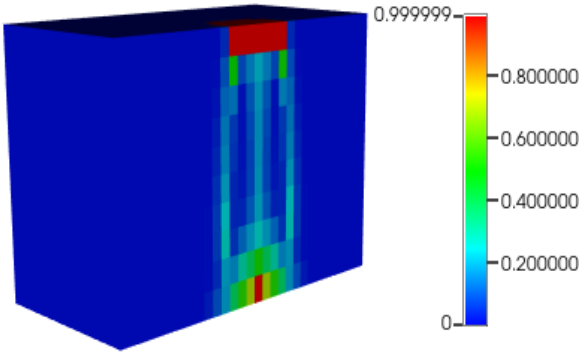

Figure 3. 3D Model for 10000 ppm

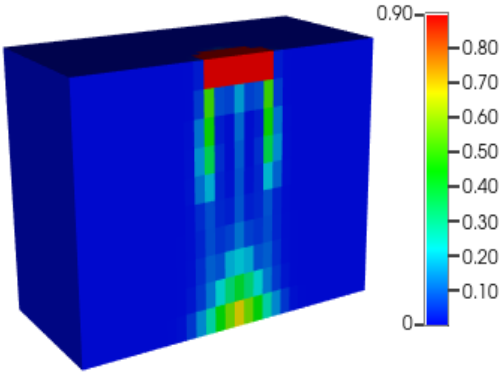

Figure 4. 3D Model for 15000 ppm

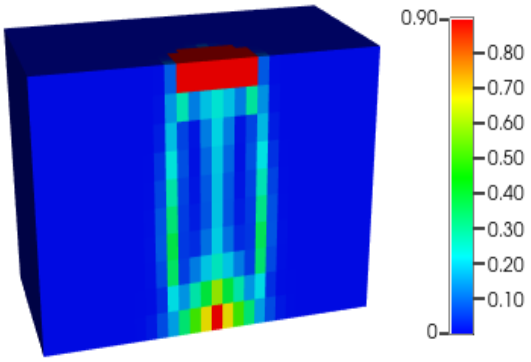

Figure 5. 3D Model for 20000 ppm

3. Results and Discussion

3.1. Amount of CO_2 Dissolved in Water

The amount of CO_2 dissolved in resident brine for pure water is presented in (Figure 6). Result reveals that a higher number of moles solubilised in the post-injection phase than the injection phase. The number of moles dissolved in the post-injection phase doubles the injection phase for each resident time. The CO_2 dissolved in moles increases with time (duration of injection) and decreases with increase in level of salinity. There was a significant difference in the CO_2 dissolved for each level of salinity with increase in time.

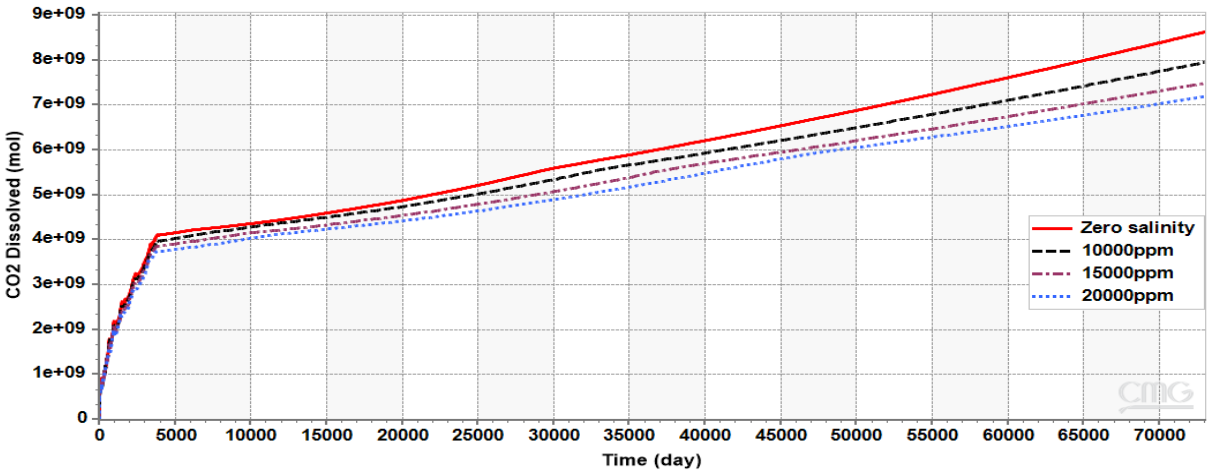

Figure 6. Aqueous Salinity on CO_2 Dissolution

3.2. Amount of CO_2 Converted to Aqueous Ions

The amount of supercritical CO_2 converted into aqueous ions, $CO_{2(aq)}$ is shown in (Figure 7). For zero salinity level, a lower number of moles of CO_2 were converted to $CO_{2(aq)}$ and later increases by one and half times the moles at 200 years. Increase in the salinity level with duration of injection decreases the level of CO_2 conversion to aqueous ion. There was no much difference between the CO_2 aqueous ions converted with increase in level of salinity for each salinity. The change in the CO_2 aqueous ions was almost the same with increase in time (duration of injection) for each level of salinity. There was a continues uniform trend for all the level of salinity with time.

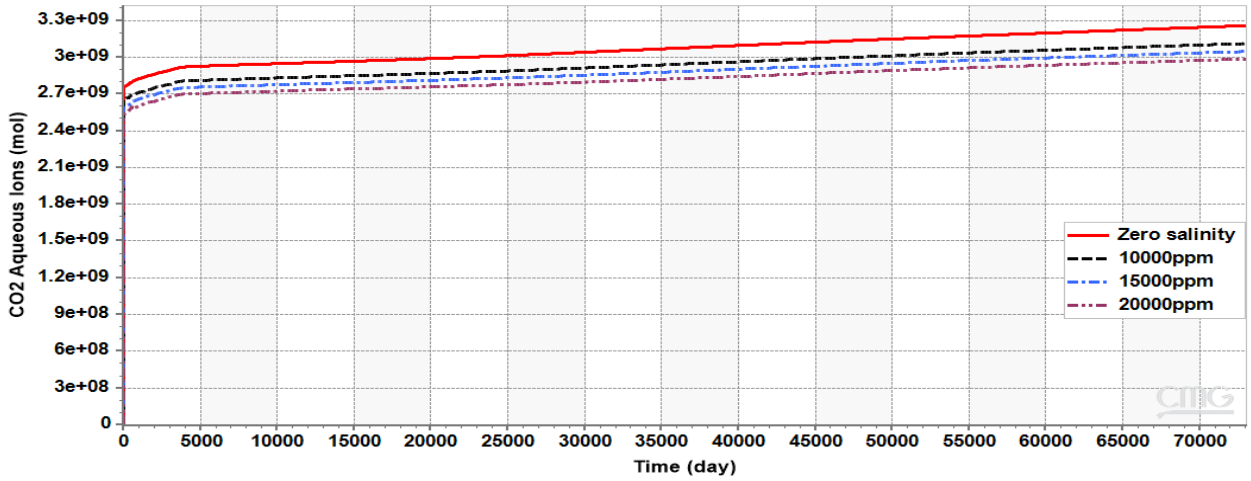

Figure 7.Aqueous Salinity on CO_2 Conversion to Aqueous Ions

3.3. Changes in Rock Mineralogy

The beginning of injection was characterised by saturation of the injected CO_2 through brine displacement away from the wellbore. Dissolution of CO_2 within formation water occurs through mass transfer from CO_2 phase to aqueous phase whenever the two phases are in contact. The dissolved CO_2 dissociates into ions, H^+ and bicarbonate, HCO_3^- and the process continues as long as there was free CO_2 phase and results in increasing HCO_3^-. The ions result in acid solutions and the possibility of attack on the initial minerals present in the formation. Resident minerals begin to dissolve as long as there is enough H^+ and generate ions (Ca^{2+} from Anorthite and Calcite, Al^{3+} from Anorthite and Kaolinite) in the system. The generated ions from the mineral dissolution process combined with bicarbonate HCO_3^- and precipitate Calcite and Kaolinite.

3.3.1. Mineral Mole Changes (Anorthite)

Changes in rock mineralogy for CO_2 injection in resident brine in the presence of various aqueous phase salinity for Anorthite are shown in (Figure 8). There was dissolution in mineral mole changes for Anorthite. The dissolution of Anorthite continue until the dissolutions of the other minerals (Calcite and Kaolinite) provide excess calcium ions (Ca^{2+}), which reverses the process to precipitation. There was a decrease in the moles of Anorthite dissolved from the injection to post-injection phase. Increase in the duration of injection decreases the mineral mole changes for each level of salinity. Increase in the level of salinity increases the mineral moles changes with time. There was a uniform decline in the mineral moles changes with increase in duration of injection.

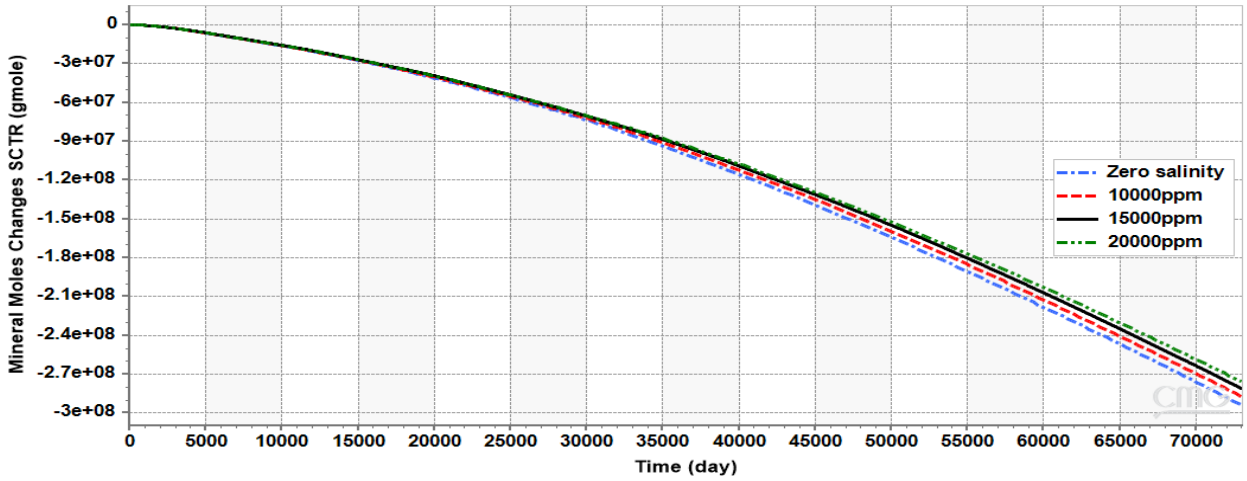

Figure 8. Aqueous Salinity on Mineral Mole Changes for Anorthite

3.3.2. Mineral Mole Changes (Calcite)

(Figure 9) shows the mineral mole changes of Calcite in resident brine of various salinities. There was continuous dissolution of Calcite minerals until the dissolution of Anorthite began to provide excess Ca^{2+} ions until precipitation occurs. The mineral mole changes of Calcite after dissolution increases with duration of injection for all salinity levels. The precipitation of Calcite (mineral mole changes) increases for all level of salinity with duration of injection. There was a uniform trend in the level of precipitation with time. Increase salinity level decreases level of Calcite precipitation.

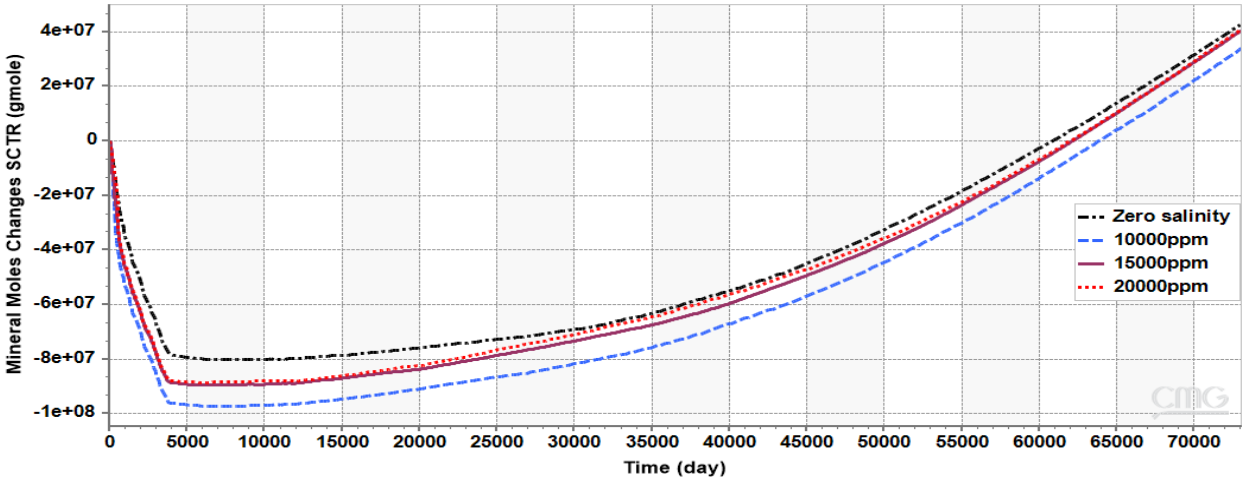

Figure 9.Aqueous Salinity on Mineral Mole Changes (Calcite)

3.3.3. Mineral Mole Mhanges (Kaolinite)

The total amount of Kaolinite precipitated in resident brine of different salinities is presented in (Figure 10). The present of excess Al^{3+} ion from Anorthite dissolution results in precipitation of Kaolinite. Increase in the level of salinity decreases the Kaolinite mineral moles changes with duration of injection. There was a uniform trend in level of Kaolinite precipitation with time. There was no significant change in mineral moles change from each level of salinity.

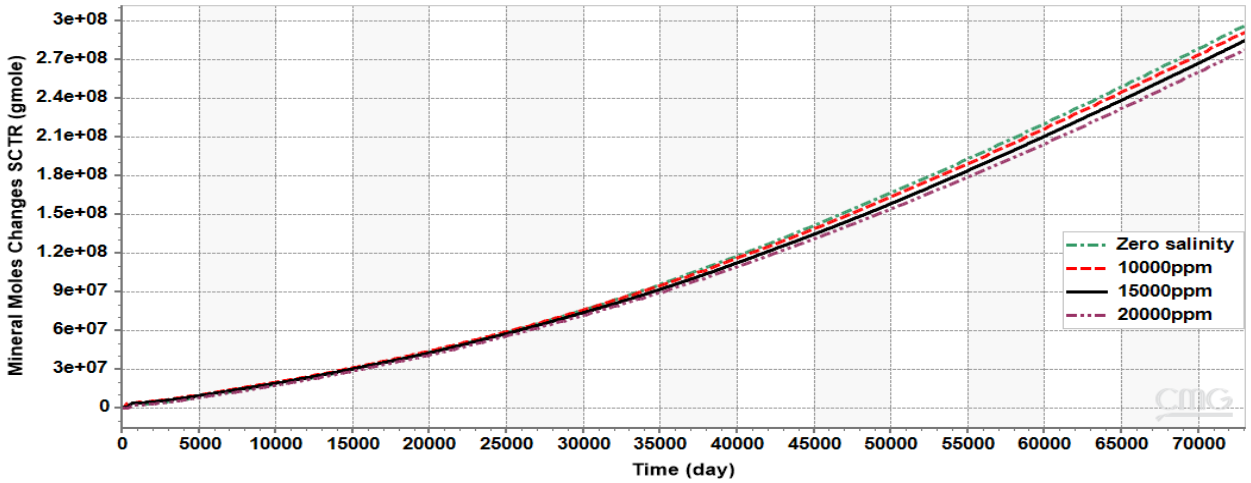

Figure 10. Aqueous Salinity on Mineral Mole Changes (Kaolinite)

3.4. Storage Capacity of CO_2 by Mineral Trapping

(Figure 11) shows aqueous phase salinities level on the storage capacity of CO_2 by mineral trapping mechanism.The results indicate a rise in the process of mineral dissolution during a period of 10 years of CO_2 injection, regardless of the salinity levels. CO_2 mineral trapped decreases with increase in level of salinity as shown in (Figure 11). While 10000 ppm gave the least CO_2 mineral trapped, 15000 ppm and 20000 ppm almost gave the same level of trapping with increase in duration of injection.

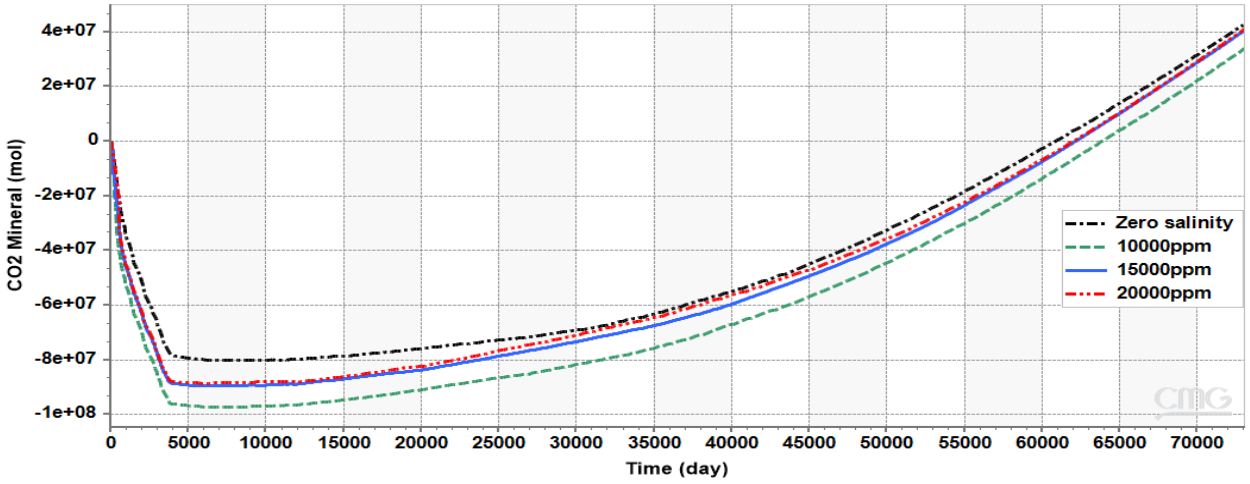

Figure 11. Aqueous Salinity on CO_2 Trapping by Mineralization

3.5.Comparison of Carbon dioxide Converted to Aqueous Ions

The carbon dioxide converted to aqueous ions for different salinity level is presented in (Figure 12). Increase in salinity level reduces the moles of carbon dioxide converted to aqueous ion.

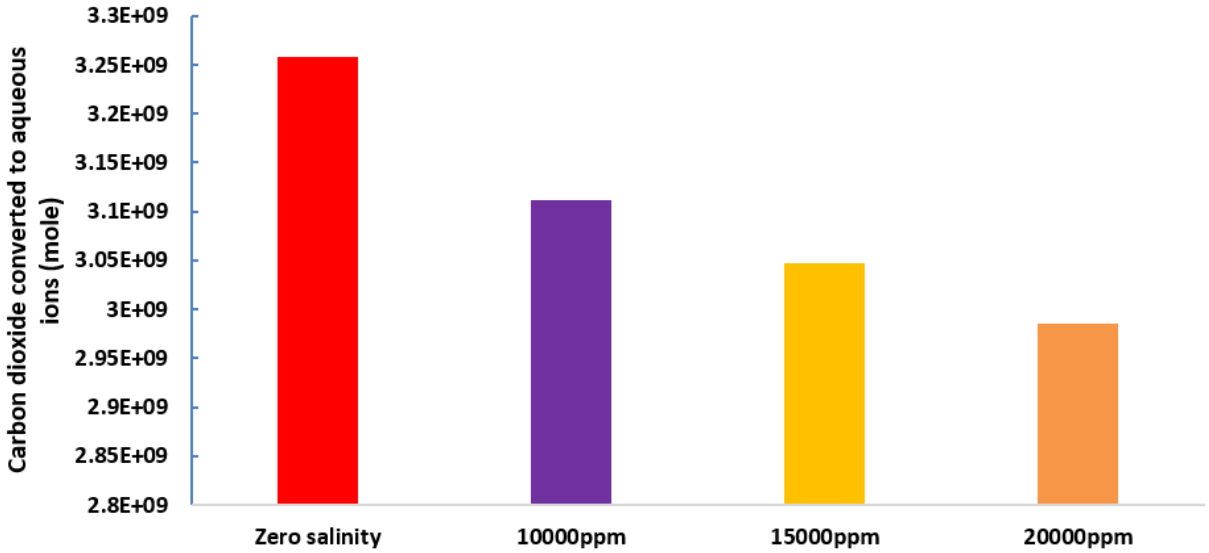

Figure 12. Carbon Dioxide Converted to Aqueous Ions for Different Salinity

3.6. Comparison of Mineral Mole Changes Due to Precipitation

The level of precipitation of the minerals for different salinities is presented in (Figure 13). Kaolinite has the highest precipitation level. The precipitation level of Kaolinite is about six(6) times the Calcite while Anorthite did not precipitate but dissolved.

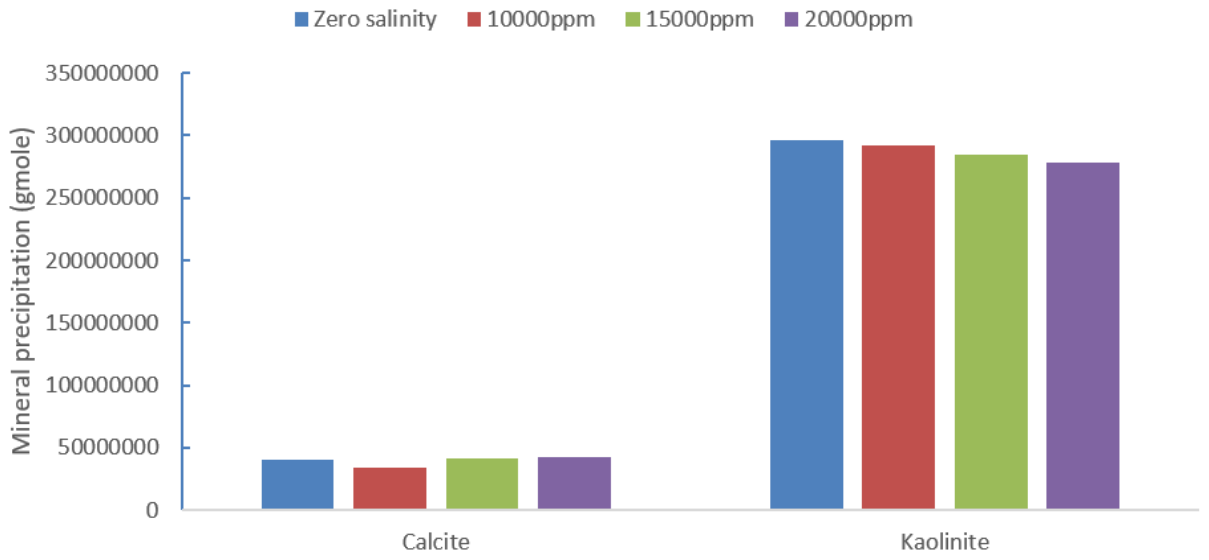

Figure 13. Precipitation Level of Minerals

3.7.Mineral Mole Changes Due to Dissolution (Anorthite)

(Figure 14) shows the mineral dissolution level at different salinities. Increase in salinity decreases the level of dissolution for Anorthite. The composition of the mineral is a vital factor for dissolution tendencies.

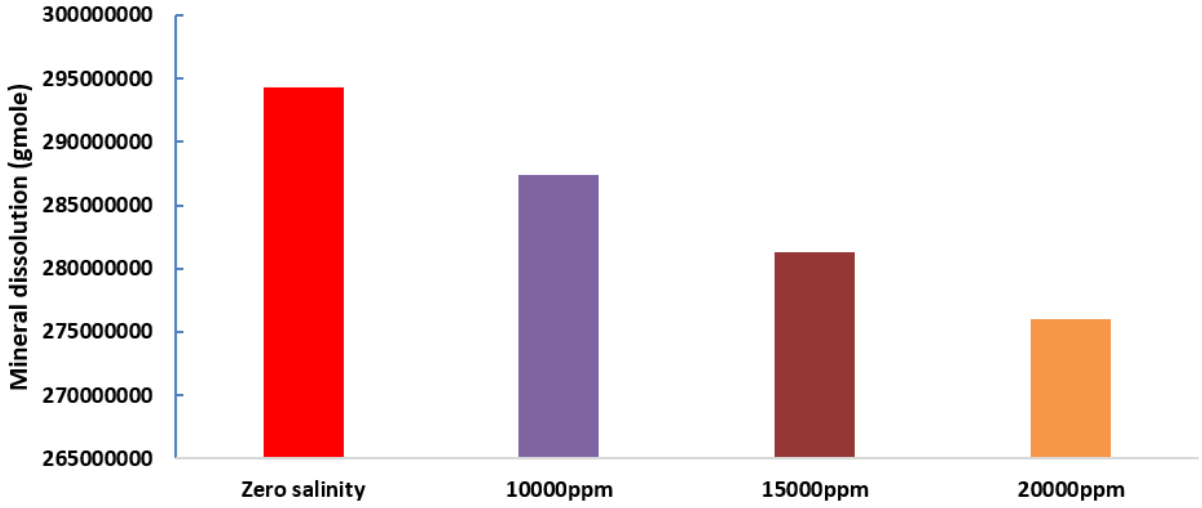

Figure 14. Mineral Dissolution Level

4. Conclusions

In this work, Numerical simulations were conducted using different salinity concentration and model outputs were compared to evaluate the affects of salinity concentrations on carbon dioxide sequestration by mineral trapping.

The following conclusions were drawn from the performed analysis:

i. The carbon dioxide dissolved in moles increases with duration of injection and decreases with increase in salinity.

ii. Increase in the salinity level with duration of injection decreases carbon dioxide conversion to aqueous ion.

iii. Increase in the level of salinity increases the mineral moles changes for Anorthite with time.

iv. Calcite precipitation rate decreases with increase in salinity level with time.

v. Kaolinite mineral moles changes decreases with increase in salinity level with duration of carbon dioxide injection.

References

Abas, N., and Khan, N. (2014). Carbon conundrum, climate change, CO_2 capture and consumptions. Journal of CO_2 Utility, 8, 39-48.

Al-Yaseri, A. Z., Lebedev, M., Barifcani, A., and Iglauer, S. (2016). Receding and advancing (CO_2 + brine + quartz) contact angles as a function of pressure, temperature, surface roughness, salt type and salinity. The Journal of Chemical Thermodynamics, 93, 416-423.

Al-khdheeawi, E.A.,Vialle, S.,Barifcani, A.,Sarmadivaleh,M.and Iglauer,S. (2017). Effect of brine salinity on CO_2 plume migration and trapping capacity in deep saline aquifers. APPEA J ,57,100-109.

Al-khdheeawi,E.A, Vialle, S.,Barifcani, A.,Sarmadivaleh,M., Zhang,Y.,and Iglauer,S. (2018).Impact of salinity on CO_2 containment security in highly heterogeneous reservoirs. Greenhouse Gases Sci Technol,8(1),93-105.

Arif, M., Al-Yaseri, A. Z., Barifcani, A., Lebedev, M., and Iglauer, S. (2016a). Impact of pressure and temperature on CO_2-brine-mica contact angles and CO_2-brine interfacial tension: implications for carbon geo-sequestration.

Journal of Colloid and Interface Science, 462, 208-215.

Bachu, S. (2016). Review of CO_2 Storage Efficiency in Deep Saline Aquifers. International Journal of Greenhouse Gas Control, 40, 188-202.

Gaus, I. (2010). Role and impact of CO_2-rock interactions during CO_2 storage in sedimentary rocks. International Journal of Greenhouse Gas Control, 4, 73-89.

Gunter, W. D., Bachu, S., and Benson, S. (2004). the role of hydrogeological and Geochemical trapping in sedimentary basins for secure geological storage of carbon dioxide. In: Geological Society of London, Special Publication, 233, 129-45.

Hesse, M., Orr, F., and Tchelepi, H. (2008). Gravity currents with residual trapping. Journal of Fluid Mechanics, 611(1), 35-60.

Iglauer, S., Al-Yaseri, A. Z., Rezaee, R., and Lebedev, M. (2015). CO_2 wettability of caprocks:Implications for structural storage capacity and containment security. Geophysical Research Letters, 42(21), 9279-9284.

Iglauer, S., Paluszny, A., Pentland, C. H., and Blunt, M. J. (2011). Residual CO_2 imaged with X- ray micro-tomography. Geophysical Research Letters, 38(21), 1-6.

Kolster, C., Agada, S., Mac Dowell, N., and Krevor, S. (2018). The impact of time-varying CO_2injection rate on large scale storage in the UK Bunter Sandstone. International Journal of Greenhouse Gas Control, 68, 77-85.

Krevor, S., Blunt, M. J., Benson, S. M., Pentland, C. H., Reynolds, C., Al-Menhali, A., and Niu, B. (2015). Capillary trapping for geologic carbon dioxide storage - from pore scale physics to field scale implications. International Journal of Greenhouse Gas Control, 40, 221-237.

Kumar, A., Noh, M. H., Ozah, R. C., Pope, G. A., Bryant, S. L., Sepehrnoori, K., and Lake, L.W. (2005). Reservoir simulation of CO_2 storage in aquifers. SPE Journal, 10(3), 336-348.

Kumar, R.,Campbell,S., Sonnenthal, E.,andCunningham,J.(2020). Effect of brine salinity on the geological sequestrationof CO_2 in a deep saline carbonate formation. Greenhouse Gas Sci Technol, 0,1-17.

Liu, B., Fu, X., and Li, Z. (2018). Impacts of CO_2-brine-rock interaction on sealingefficiency of sand caprock: a case study of Shihezi formation in Ordos basin. Advances in Geo-Energy Research, 2, 380-392.

Naylor, M., Wilkinson, M., and Haszeldine, R. (2011). Calculation of CO_2 column heights in depleted gas fields from known pre-production gas column heights. Marine Petroleum Geology, 28(5), 1083-1093.

Olajire, A. A. (2018). Recent progress on the nanoparticles-assisted greenhouse carbon dioxide conversion processes. Journal of CO_2 Utility, 24, 522-547.

Pentland, C. H., El-Maghraby, R., Iglauer, S., and Blunt, M. J. (2011). Measurements of the capillary trapping of super-critical carbon dioxide in Berea sandstone. Geophysical Research Letters, 38(6), 1-4 .

Pruess, K., Xu, T., Apps, J., and Garcia, J. (2003). Numerical modelling of aquifer disposal of CO_2. SPE Journal, 8(1), 49-60.

Rahman, T., Lebedev, M., Barifcani, A., and Iglauer, S. (2016). Residual trapping of supercritical CO_2 in oil-wet sandstone. Journal of Colloid and Interface Science, 469, 63- 68.

Saraji, S., Piri, M., and Goual, L. (2014). The effects of SO_2 contamination, brine salinity,pressure, and temperature on dynamic contact angles and interfacial tension of supercritical CO_2/ brine/quartz systems. International Journal of Greenhouse Gas Control, 28, 147-155.

Singh, H. (2018). Impact of four different CO_2injection schemes on extent of reservoir pressure and saturation. Advances in Geo-Energy Research, 2, 305-318.

Spycher, N., Pruess, K., and Ennis-King, J. (2003). CO_2-H_2O mixtures in the geological sequestration of CO_2. Assessment and calculation of mutual solubilities from 12 to 100 °C and up to 600bar. Geochimica et Cosmochimica Acta, 67(16), 3015-3031.

Venkatraman, V., and Alsberg, B. K. (2017). Predicting CO_2 capture of ionic liquids using machine learning. Journal of CO_2 Utility, 21, 162-168.

Xu, T., Apps, J. A., and Pruess, K. (2003). Reactive geochemical transport simulation to study mineral trapping for CO_2 disposal in deep arenaceous formations. Journal of Geophysical Research: Solid Earth, 108(B2), 1-13.

Xu, T., Apps, J. A., and Pruess, K. (2004). Numerical simulation of CO_2 disposal by mineral trapping in deep aquifers. Applied Geochemistry, 19(6), 917-936.

Xu, T., Apps, J. A., and Pruess, K. (2005). Mineral sequestration of carbon dioxide in a sandstone-shale system. Chemical Geology, 217(3), 295-318.

Zhang, Y., Lebedev, M., Sarmadivaleh, M., Barifcani, A., and Iglauer, S. (2016). Swelling-induced changes in coal microstructure due to supercritical CO_2 injection. Geophysical Research Letter 43(17), 9077-9083.

ارزیابی تأثیر شوری فاز آبی بر معدنی شدن دی‌اکسید کربن در طول فرآیند ذخیره‌سازی گاز

- برایات بریاکپوآ کیناته[1,*]، اوگونا دیکسون آمادی[2]، اولالکان کونل آکیندله[3]، جرمیاه ایفئانی اکرومه[4]

۴،۱. گروه مهندسی نفت، دانشگاه ایالتی ریورز، پورت هارکورت، نیجریه

۲. گروه نفت و گاز، دانشگاه سالفورد، منچستر، انگلستان

۳. گروه علوم داده، هوش مصنوعی و مدل‌سازی، دانشگاه هال، انگلستان

(ایمیل نویسنده مسئول: ahhassani@srb.iau.ir)

چکیـــــــده

در این پژوهش، تأثیر شوری فاز آبی بر فرآیند معدنی شدن دی‌اکسید کربن بررسی شده است. شوری فاز آبی تأثیر قابل توجهی بر میزان دی‌اکسید کربن به دام افتاده از طریق مکانیزم انحلالی دارد و همچنین ممکن است بر فرآیندهای انحلال و رسوب‌گذاری مواد معدنی تأثیر بگذارد. در حالی که روش‌های مختلف ذخیره‌سازی دی‌اکسید کربن از جمله ذخیره‌سازی ساختاری، باقیمانده، انحلالی و تا حدی معدنی به طور گسترده مطالعه شده‌اند، پتانسیل به دام‌اندازی معدنی و عوامل مؤثر بر آن کمتر مورد بررسی قرار گرفته‌اند. در این تحقیق، تأثیر تغییرات شوری فاز آبی بر معدنی شدن دی‌اکسید کربن از طریق شبیه‌سازی عددی بررسی شده است. این شبیه‌سازی با استفاده از یک شبیه‌ساز ژئوشیمیایی و یک مدل سه‌بعدی همگن از یک آبخوان با ابعاد ۰۱×۰۳×۰۳ (۰۰۰۹ بلوک شبکه‌ای) و عرض هر بلوک ۰۷ متر انجام شده است. شبکه تولید شده با ویژگی‌های پتروفیزیکی، شبکه‌بندی و خصوصیات سنگی پر شده است. چهار مدل با خصوصیات سنگ و سیال مشابه برای شرایط آب خالص و شوری‌های مختلف (۱۰۰۰۰ppm) ۰،۰۱ wt (۱۵۰۰۰ppm) ۰،۰۱۵ wt و (۲۰۰۰۰ppm) ۰،۰۲ wt به ترتیب شبیه‌سازی شدند. نتایج نشان داد که با افزایش شوری آب شور، میزان دی‌اکسید کربن حل‌شده کاهش می‌یابد. افزایش شوری باعث کاهش مول‌های دی‌اکسید کربن تبدیل‌شده به یون‌های محلول در آب و کاهش میزان انحلال در آب موجود می‌شود. همچنین، با افزایش مدت زمان تزریق دی‌اکسید کربن، نرخ رسوب‌گذاری کائولینیت و کلسیت افزایش یافته، در حالی که نرخ انحلال آنورتیت کاهش می‌یابد. تغییرات مولی مواد معدنی در مورد آنورتیت با افزایش سطح شوری افزایش یافته اما با افزایش مدت زمان تزریق دی‌اکسید کربن کاهش می‌یابد. از سوی دیگر، تغییرات مولی کلسیت و کائولینیت با افزایش سطح شوری و مدت زمان تزریق کاهش پیدا می‌کند. به طور کلی، با افزایش شوری فاز آبی، مقدار کلسیت و کائولینیت کاهش می‌یابد.

این مطالعه نشان داده است که واکنش‌پذیری مواد معدنی تشکیل‌دهنده مخزن نسبت به غلظت شوری متفاوت است که این امر نقش تعیین‌کننده‌ای در ظرفیت ذخیره‌سازی و به دام‌اندازی دی‌اکسید کربن دارد.

واژگان کلیدی: معدنی شدن، انحلال، مدل آبخوان، شوری فازی، ذخیره‌سازی